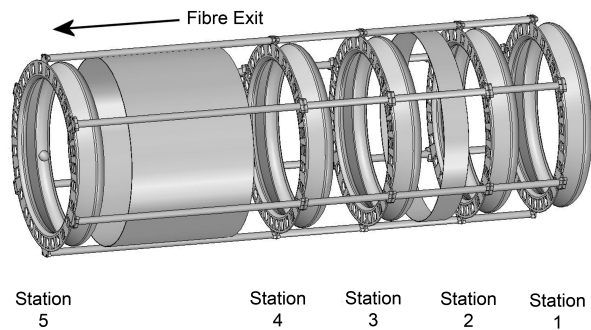


MICE TRACKER SOFTWARE DOCUMENTATION

The MICE tracker software team



January 8, 2013

Contents

1. Introduction	1
2. Definitions	1
2.1. Labelling of upstream and downstream trackers	1
2.2. Station numbering	1
2.3. Doublet layer	1
2.4. Fibre-channel numbering	3
3. Reference surfaces and coordinate systems	4
3.1. Doublet layer	4
3.2. Station	4
3.3. Tracker	5
3.4. Coordinate transformations	6
4. Reconstruction	6
4.1. Hits and clusters	6
4.2. Space-point reconstruction	8
4.3. Pattern recognition	10
4.4. Track fit	16
5. Data structure	16
6. Algorithms	16
6.1. General Code Structure	17
7. Configuration data base	17
8. Monte Carlo	18
9. Performance	18
A. Kuno's Conjecture	20
B. Space-point variance	21
C. Circle parameters from three points	24
D. Circle fit	26

1. Introduction

This document describes the implementation of the software used to simulate and to reconstruct the MICE scintillating fibre trackers. Detailed descriptions of the trackers may be found in [? ? ?] and will not be repeated here.

2. Definitions

2.1. Labelling of upstream and downstream trackers

The labels for two trackers are:

Upstream tracker → Tracker#1

Downstream tracker → Tracker#2

2.2. Station numbering

The TRD [?] defines the station “labelling” of the stations in relation to the focus-coil module that is immediately downstream of tracker 1 or, equivalently, immediately upstream of tracker 2. The station closest to the focus-coil module in question is labelled “1”. The label then increases such that station 5 is the station closest to the optical patch panel. The scheme is summarised in table I and figure 1.

TABLE I. Station numbering scheme. The “label” of the stations that make up a MICE tracker runs from 1 to 5. The location of the station in relation to the patch panel and the absorber is reported in the column labelled “Location”.

Location	Label
Closest to absorber (furthest from patch panel)	1
	2
	3
	4
Furthest from absorber (closest to patch panel)	5

2.3. Doublet layer

Each station consists of three “doublet layers” of $350\mu\text{m}$ scintillating fibres glued onto a carbon-fibre station body. The doublet layers are arranged such that the fibres in one layer run at an angle of 120° to the fibres in each of the other layers as shown in figure 2a. The arrangement of the fibres within a doublet layer is shown in figure 2b. The configuration of the seven fibres ganged for readout via a single clear-fibre light-guide is also indicated. The construction of the doublet layer is described in [?] along with the specification of the various materials of which it is composed.

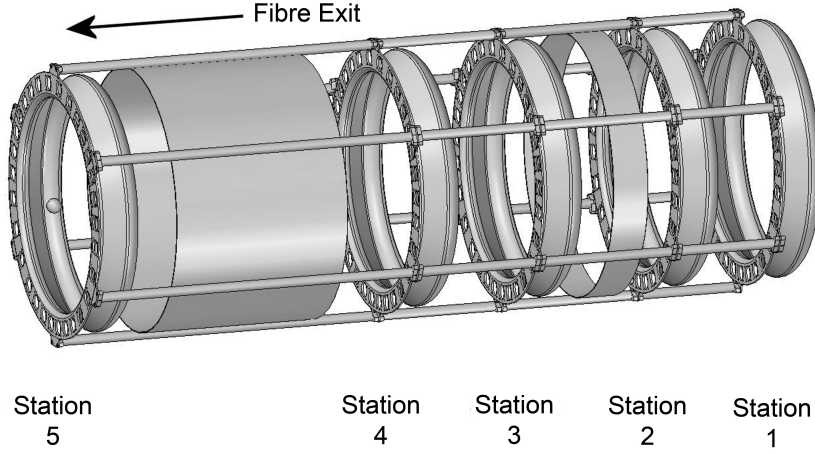


FIG. 1. Schematic diagram of the MICE tracker. The five stations are shown supported by the carbon-fibre space frame, with bres omitted for clarity. The station numbering scheme is indicated together with the direction in which the clear-fibre light-guides leave the tracking volume.

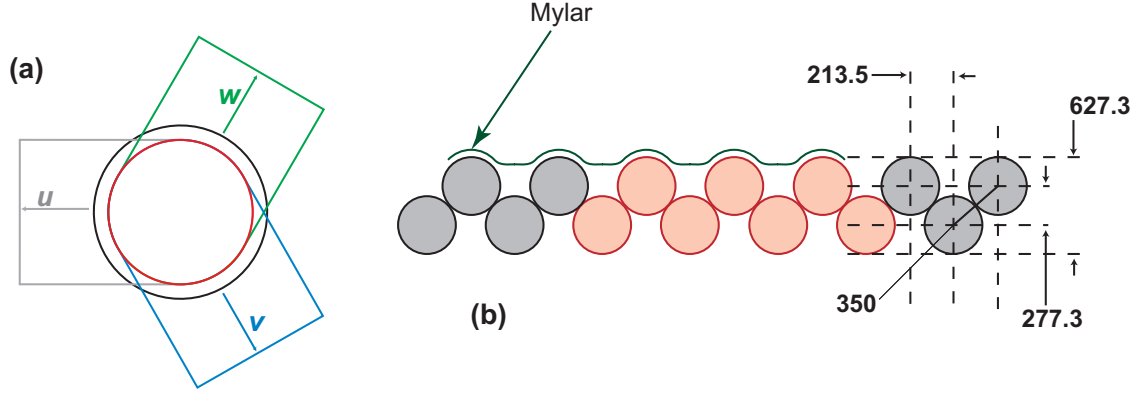


FIG. 2. (a) Arrangement of the doublet layers in the scintillating-fibre stations. The outer circle shows the solenoid bore while the inner circle shows the limit of the active area of the tracker. The grey, blue, and green regions indicate the direction that the individual $350\ \mu\text{m}$ fibres run (moving outward from the centre) in the u , v , and w planes respectively. (b) Detail of the arrangement of the scintillating fibres in a doublet layer. The fibre spacing and the fibre pitch are indicated on the right-hand end of the figure in μm . The pattern of seven fibres ganged for readout in a single clear-fibre light-guide is shown in red. The sheet of Mylar glued to the doublet layer is indicated.

2.3.1. Doublet-layer numbering

The order in which the doublet layers were glued onto the station body is shown in figure 3. The u layer was glued to the station body first. The doublet layer was glued such that the “fibre side” of the doublet layer was glued to the station body; i.e. the mylar sheet faces away from the station body. The w layer was then glued onto the outer surface of the u layer. The fibre side of the w layer was glued to the mylar sheet of the u layer such that the mylar sheet of the “ w ” layer also faces away from the station body.

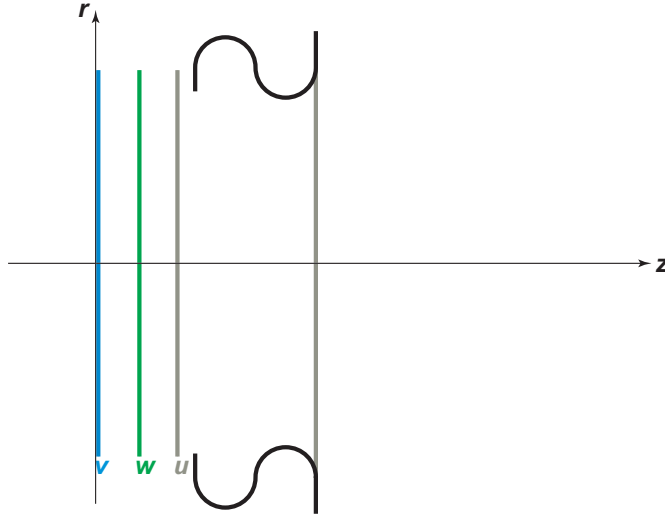


FIG. 3. The order in which the doublet layers were glued onto the station body. The station body is indicated by the solid black lines. The u layer (shown as the grey line) was glued to the station body first. The w (indicated by the green line) was then glued onto the outer surface of the u layer. The outer doublet layer, the v layer (shown as the blue line) was then glued onto the assembly. The station reference surface and the direction of increasing z are shown as the thin black lines.

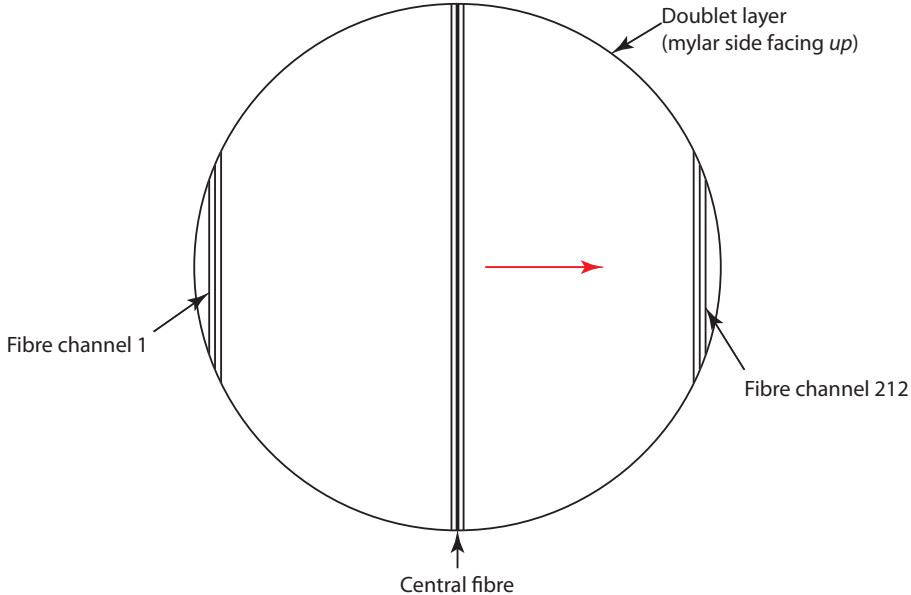
TABLE II. Doublet-layer numbering scheme. The doublet-layer “number” runs from 0 to 2. The correspondance between the doublet layer number and the view is reported in the column labelled “Doublet-layer number”.

View	Double-layer number
u	0
w	1
v	2

Finally, the v layer was glued onto the assembly. The gluing arrangement was the same as for the u and w layers, i.e. the mylar sheet of the v layer also faces away from the station body. The numbering of the layers, which follows the order in which the layers were glued onto the station body, is summarised in table II.

2.4. Fibre-channel numbering

The numbering of the groups of seven fibres ganged for readout is shown in figure 4. With the mylar surface facing up, and with the tails leading out to the station connectors taken to be at the bottom of the figure, the fibre-channel increases from left to right. The coordinate measured by the doublet layer (u , v or w) is taken to increase in the same direction as the channel number. The origin of the measured coordinate is taken to be at the position of the central fibre.



Fibre run to the station optical connectors taken to be towards the bottom of the figure.

FIG. 4. The order in which fibre channels (groups of seven fibres) are numbered. The sensitive surface of the doublet layer is indicated by the solid circle. The direction in which the fibres run is indicated by the vertical lines. The station optical connectors are taken to be at the bottom of the figure as indicated. With the mylar sheet taken to be facing up, fibre-channel number 1 is to the left of the central fibre. The fibre-channel number increases from left to right. The “zero” of the coordinate (u , v or w increases) measured by the doublet layer is taken to be the position of the central fibre. The direction in which the coordinate measured by the doublet layer increases is indicated by the red arrow.

3. Reference surfaces and coordinate systems

3.1. Doublet layer

The doublet-layer reference surface is defined to be the flat plane that is tangential to the outer surface of the mylar plane as shown in Figure 5a. The measured coordinate, $\alpha \in u, v, w$, is defined to lie in this plane and the α axis is perpendicular to the direction in which the fibres run. The doublet-layer z_d axis is defined to be perpendicular to the doublet-layer reference surface increasing in the direction indicated in the figure. The direction in which the measured coordinate, α increases is indicated in figure 5b. The orthogonal coordinate in the doublet-layer reference surface that with α and z_d completes a right handed coordinate system is referred to as β . The β axis is also indicated in figure 5b.

3.2. Station

The station reference surface is defined to coincide with the reference surface of the v doublet layer (see figure 6). The station coordinate system is defined such that the y_s axis is coincident with v axis, the z_s axis is coincident with the z_d axis of the v layer and the x_s axis completes a right-handed coordinate

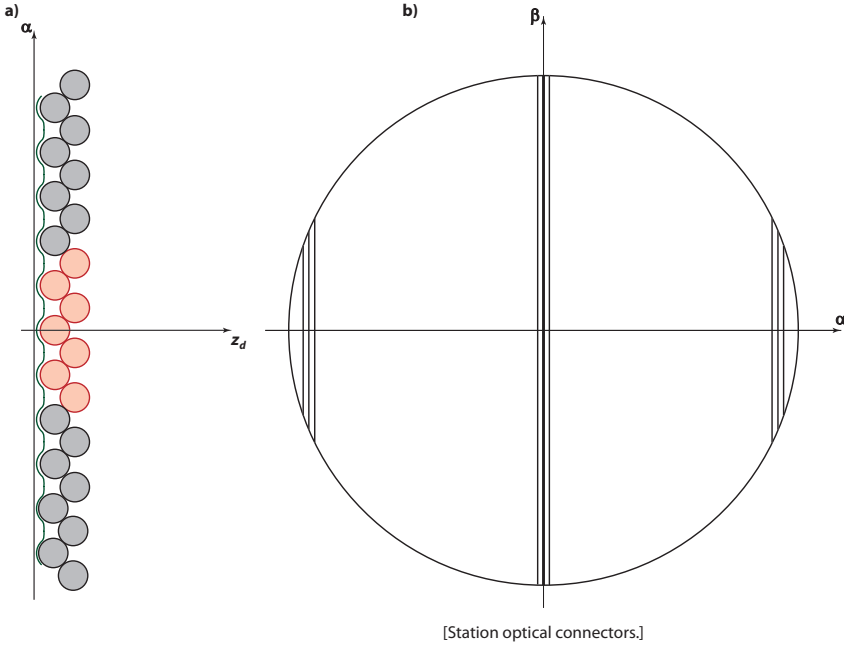


FIG. 5. Reference surfaces and coordinate-system definitions for the doublet layer and station. a) The fibres in the doublet layer are shown as the shaded circles, the central channel being shaded pink. The mylar layer is indicated by the solid black corrugated line. The doublet-layer reference surface is indicated by the vertical straight line, the arrow labelled α indicates the direction in which the coordinate measured by the doublet layer (u , v or w) increases. The direction of the z_d axis is indicated. b) View of doublet layer looking down on the mylar layer with the optical connectors at the bottom of the figure. The coordinate measured by the doublet layer (u , v or w) is indicated by the axis labelled α . The orthogonal axis, i.e. the direction in which the fibres run, is labelled β . The origin of the (α, β) coordinate system is taken to be at the centre of the circular active area.

system.

3.3. Tracker

The tracker reference surface is defined to coincide with the reference surface of station 1. The tracker coordinate system is defined such that the z_t axis coincides with the nominal axis of cylindrical symmetry of the tracker as shown in figure 7. The tracker z_t coordinate increases from station 1 to station 5. The tracker y_t axis is defined to coincide with the y_s axis of station 1 and the tracker x_t axis completes a right-handed coordinate system.

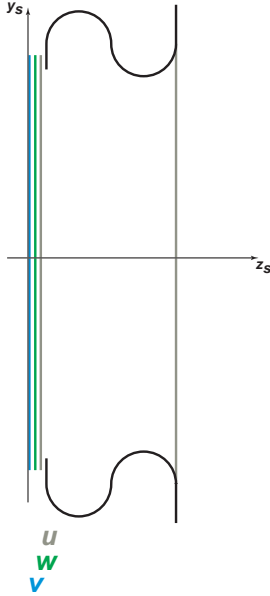


FIG. 6. The carbon-fibre station body is indicated by the heavy solid black lines. The three doublet layers are indicated by the solid grey (u), green (w) and blue (v) lines. The station reference surface is shown by the solid vertical line coincident with the reference surface of the doublet layer labelled v . The direction y_s axis, defined to be coincident with the v axis and the z_s axes are shown as the solid, black arrows. The x_s axis completes a right-handed coordinate system and therefore points into the page.

3.4. Coordinate transformations

3.4.1. Doublet-layer to station

The transformation from doublet-layer to station coordinates is achieved using the rotation $\underline{\underline{R}}_{SD}$ defined by:

$$\mathbf{r}_s = \begin{pmatrix} x_s \\ y_s \end{pmatrix} = \underline{\underline{R}}_{SD} \mathbf{m} = \begin{pmatrix} \cos \theta_D & -\sin \theta_D \\ \sin \theta_D & \cos \theta_D \end{pmatrix} \begin{pmatrix} \alpha \\ \beta \end{pmatrix}; \quad (1)$$

where θ_D is the angle which the fibres that make up the doublet-layer make to the x_s axis in the station coordinate system.

4. Reconstruction

4.1. Hits and clusters

A track passing through a particular doublet layer produces scintillation light in one or at most two fibre channels. For each channel ‘hit’, the tracker data acquisition system records the channel number, n , and the pulse height. After calibration, the pulse height is recorded in terms of the number of photo-electrons (n_{pe}) generated in the Visible Light Photon Counter (VLPC) illuminated by the hit channel.

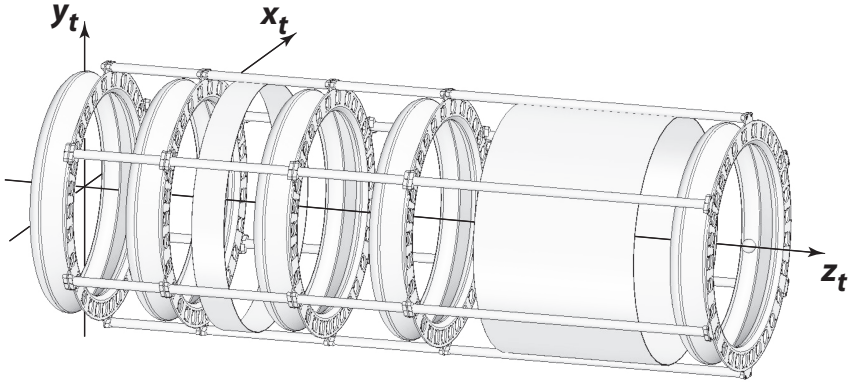


FIG. 7. The outline of the components that make up the MICE tracker are shown in the line drawing. The tracker reference surface coincides with the reference surface of station 1. The tracker coordinate system is indicated by the solid lines. The y_t axis is defined to be coincident with the y_s axis in the station coordinate system. The z_t axis runs along the nominal axis of the tracker. The x_t axis completes a right-handed coordinate system.

Occasionally, showers of particles or noise can cause three or more neighbouring channels to be hit. The term “clusters” is used to refer to an isolated hit, a doublet cluster and a multi-hit cluster.

The position of a hit in the doublet-layer coordinate system may be determined from the channel number. For isolated hits, the measured coordinate $\alpha \in u, v, w$ is given by:

$$\alpha = c_p(n - n_0); \quad (2)$$

where n_0 is the channel number of the central fibre and c_p is the channel pitch given by:

$$c_p = 3f_p + f_d \quad (3)$$

where f_d is the fibre diameter ($f_d = 350 \mu\text{m}$) and f_p is the fibre pitch ($f_p = 427 \mu\text{m}$ see figure 2). For clusters in which two channels are hit (“doublet clusters”, see figure 8), the measured coordinate is given by:

$$\alpha = c_p \left[\frac{(n_1 + n_2)}{2} - n_0 \right]; \quad (4)$$

where n_1 and n_2 are the channel numbers of the two hit fibres. For a multi-hit cluster (clusters with more than two neighbouring channels), the measured position is determined from the pulse-height weighted mean of the fibre positions:

$$\alpha = c_p \left[\frac{\sum_i n_{\text{pe}i} n_i}{\sum_i n_{\text{pe}i}} \right]; \quad (5)$$

where the subscript i indicates the i^{th} channel. The pulse-height for doublet and multi-channel clusters is determined by summing the pulse height of all the hits that make up the cluster.

The “measurement vector”, \mathbf{m} is defined as:

$$\mathbf{m} = \begin{pmatrix} \alpha \\ \beta \end{pmatrix}; \quad (6)$$

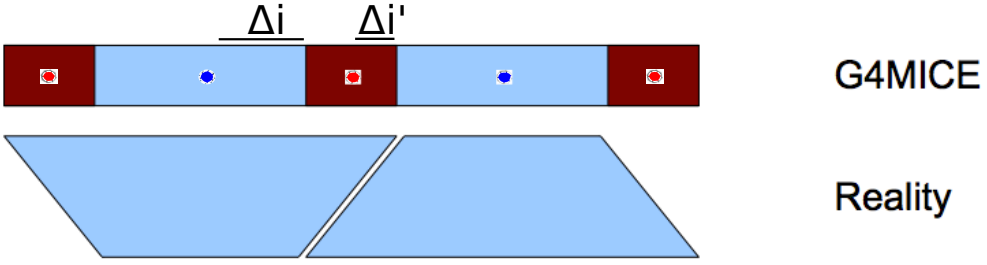


FIG. 8. Channel overlap as simulated in G4MICE; fine-tuning reduces the error associated to doublet clusters.

where α is given above and, in the absense of additional information, $\beta = 0$. The corresponding covariance matrix is given by:

$$\underline{\underline{V}_m} = \begin{pmatrix} \sigma_\alpha^2 & 0 \\ 0 & \sigma_\beta^2 \end{pmatrix}; \quad (7)$$

where σ_α^2 and σ_β^2 are the variance of α and β respectively. The variance on α for a single-hit cluster is given by:

$$\sigma_m^2 = \frac{c_p^2}{12}. \quad (8)$$

For a doublet-cluster, the variance is given by:

$$\sigma_m^2 = \frac{\Delta_\alpha^2}{12}; \quad (9)$$

where $\Delta_\alpha = ?$ is the length of the overlap region between neighbouring fibre channels (see figure 8). For multihit clusters, the variance is given by

$$\sigma_m^2 = \frac{??}{??}. \quad (10)$$

The variance of the perpendicular coordinate, β , depends on the effective length, l_{eff} of the fibre (see figure ?? and Appendix ??) and is given by:

$$\sigma_\beta^2 = \frac{l_{\text{eff}}^2}{12}; \quad (11)$$

where

$$l_{\text{eff}} = ?? . \quad (12)$$

4.2. Space-point reconstruction

This section describes the space-point reconstruction, the algebra by which the cluster positions are translated in to tracker coordinates and, to some extent, the algorithm.

4.2.1. Selection of clusters that form the space-point

For each particle event, the clusters found within each doublet layer are ordered by fibre-channel number. Taking each station in turn, an attempt is made to generate a space point using all possible combinations of clusters. The three clusters, one each from views u , v and w , that make up a space point satisfy:

$$n^u + n^v + n^w = n_0^u + n_0^v + n_0^w; \quad (13)$$

where n^u , n^v and n^w are the fibre numbers of the clusters in the u , v and w views respectively and n_0^u , n_0^v and n_0^w are the respective central-fibre numbers (see Appendix A). A triplet space point is selected if:

$$|(n^u + n^v + n^w) - (n_0^u + n_0^v + n_0^w)| < K. \quad (14)$$

Once all triplet space-points have been found, doublet space-points are created from pairs of clusters from different views.

4.2.2. Crossing-position calculation

4.2.2.1. Doublet space-points

The position of the doublet space-point in station coordinates, \mathbf{r}_s , is given by:

$$\mathbf{r}_s = \begin{pmatrix} x_s \\ y_s \end{pmatrix} \quad (15)$$

$$= \underline{\underline{R}}_{SD1} \mathbf{m}_1 \quad (16)$$

$$= \underline{\underline{R}}_{SD2} \mathbf{m}_2; \quad (17)$$

where the measurement vector corresponding to the i^{th} cluster:

$$\mathbf{m}_i = \begin{pmatrix} \alpha_i \\ \beta_i \end{pmatrix}; \quad (18)$$

and the rotation matrix $\underline{\underline{R}}_{SDi}$ are defined in section 4.1. The simultaneous equations 16 and 17 contain two unknowns, β_1 and β_2 . Equations 16 and 17 may be rewritten:

$$\mathbf{m}_1 = \underline{\underline{R}}_{SD1}^{-1} \underline{\underline{R}}_{SD2} \mathbf{m}_2. \quad (19)$$

Defining:

$$\underline{\underline{S}} = \underline{\underline{R}}_{SD1}^{-1} \underline{\underline{R}}_{SD2} \quad (20)$$

$$= \begin{pmatrix} s_{11} & s_{12} \\ s_{21} & s_{22} \end{pmatrix}; \quad (21)$$

equations 16 and 17 may be solved to yield:

$$\beta_2 = \frac{\alpha_1 - s_{11}\alpha_2}{s_{12}} \quad (22)$$

$$\beta_1 = s_{21}\alpha_2 + s_{22}\beta_2. \quad (23)$$

The position of the space-point may now be obtained from equation 16 or 17.

4.2.2.2. Triplet space-points

As shown in figure 13, the fibres layout is of one of two types. In one case (right panel of figure 13), the centre of the channels, one in each of the three views, cross intersect at a single point. In this case, the position of the crossing can be calculated as described in section 4.2.2.1. When the area of overlap of the three channels forms a triangle (figure 13 left panel), the centre of area of overlap is given by:

$$\bar{x} = \frac{2}{3}c_p; \text{ and} \quad (24)$$

$$\bar{y} = 0. \quad (25)$$

4.3. Pattern recognition

4.3.1. Straight-line pattern recognition

In the absense of a magnetic field, the tracks passing through the tracker may be described using a straight line in three dimensions. Taking the z coordinate as the independent parameter, the track parameters may be taken to be:

$$\mathbf{v}^{\text{sl}} = \begin{pmatrix} x_0 \\ y_0 \\ t_x \\ t_y \end{pmatrix}; \quad (26)$$

where, x_0 and y_0 are the position at which the track crosses the tracker reference surface, $t_x = \frac{dx}{dz}$ and $t_y = \frac{dy}{dz}$. The track model may then be written:

$$x = x_0 + zt_x; \text{ and} \quad (27)$$

$$y = y_0 + zt_y. \quad (28)$$

Pattern recognition then procedes as follows. A space-point is chosen in each of two stations, i and j where i and j label two different stations and $j > i$. Ideally, $i = 1$ and $j = 5$. However, a search of all combinations of pairs for which $j - i > 1$ is made, taking the pairs in the order of decreasing separation in z ; i.e. in order of decreasing $\Delta z_{ji} = z_j - z_i$. Initial values for the track parameters,

$$\mathbf{v}_{\text{Init}}^{\text{sl}} = \begin{pmatrix} x_0^{\text{Init}} \\ y_0^{\text{Init}} \\ t_x^{\text{Init}} \\ t_y^{\text{Init}} \end{pmatrix}, \quad (29)$$

are then calculated as follows:

$$t_x^{\text{Init}} = \frac{x_j - x_i}{z_j - z_i}; \quad (30)$$

$$x_0^{\text{Init}} = x_i - z_i t_x^{\text{Init}}; \quad (31)$$

$$t_y^{\text{Init}} = \frac{y_j - y_i}{z_j - z_i}; \text{ and} \quad (32)$$

$$y_0^{\text{Init}} = y_i - z_i t_y^{\text{Init}}; \quad (33)$$

where (x_i, y_i, z_i) are the coordinates of space-point i , etc. A search is then made for space-points in each of the stations, k , between station i and station j . The distance between the x and y coordinates of the space-points in the stations k ; $j < k < i$ and the line defined by the initial track parameters is then calculated at the reference surface of station k as follows:

$$\delta x_k = x_k - (x_0^{\text{Init}} + z_k t_x^{\text{Init}}) \text{ and} \quad (34)$$

$$\delta y_k = y_k - (y_0^{\text{Init}} + z_k t_y^{\text{Init}}). \quad (35)$$

Points are accepted as part of a “trial” track if:

$$|\delta x_k| < \Delta_x \text{ and} \quad (36)$$

$$|\delta y_k| < \Delta_y. \quad (37)$$

If at least one space-point satisfies this selection, a “trial track” is formed consisting of the space-points selected in stations i, k, \dots and j .

For each “trial track”, a straight-line fit is performed to calculate the fit χ^2 :

$$\chi^2 = \chi_x^2 + \chi_y^2. \quad (38)$$

Expressions for the evaluation of χ_x^2 and χ_y^2 are given in Appendix ???. If the fit χ^2 satisfies:

$$\frac{\chi^2}{N-2} < \chi_{\text{cut}}^2, \quad (39)$$

then the trial track is accepted and the pattern-recognition track parameters and covariance matrix are calculated using the expressions given in Appendix ??.

4.3.2. Helix pattern recognition

4.3.2.1. Helix parameters

In the presence of a magnetic field, the tracks passing through the tracker may be described using a helix. In tracker coordinates, the tracks form circles in the (x, y) plane. Defining s to be the length of the arc swept out by the track in the (x, y) plane, a track may be described using a straight line in the (s, z) plane. Taking the z coordinate as the independent parameter, the track parameters may be taken to be:

$$\mathbf{v}^{\text{hlx}} = \begin{pmatrix} x_0 \\ y_0 \\ \psi_0 \\ t_s \\ \rho \end{pmatrix}; \quad (40)$$

where, x_0 and y_0 are the position at which the track crosses the tracker reference surface, ψ_0 is the azimuthal angle of the line tangent to the track in the (x, y) plane, $t_s = \frac{ds}{dz}$ and ρ is the radius of curvature. The angle ψ_0 is chosen such that:

$$\hat{\psi}_0 = \hat{\mathbf{k}} \times \hat{\mathbf{r}}; \quad (41)$$

where $\hat{\mathbf{r}}$ is the unit vector in the direction (x_0, y_0) and $\hat{\mathbf{k}}$ is the unit vector parallel to the z axis. $\hat{\psi}_0$ is the unit vector tangent to the track and in the direction is defined by ψ_0 . With this definition, the projection on the (x, y) plane of a positive track propagating in the positive z direction sweeps anticlockwise.

4.3.2.2. Track model for pattern recognition

To build up the track model, consider a track-based coordinate system which has its origin at the point (x_0, y_0) and in which the x' axis is parallel to the line joining (x_0, y_0) to the centre of the circle described by the track, the y' axis is parallel to $\hat{\psi}_0$ and the z' axis is parallel to \hat{k} (see figure 9).

A point, i , on the track at (x_i, y_i) (tracker coordinates) at which the track direction is ψ_i may be used to write down the track model as:

$$x'_i = \rho[\cos \phi'_i - 1] \text{ and} \quad (42)$$

$$y'_i = \rho \sin \phi'_i; \quad (43)$$

where:

$$\tan \frac{\phi'_i}{2} = \frac{\sqrt{(x_i - x_0)^2 + (y_i - y_0)^2}}{2\rho}. \quad (44)$$

The z coordinate is taken as a parameter since the construction of the trackers ensures that each reference surface (tracker, station or doublet layer) is at a well defined z . The distance travelled in the (x, y) plane to reach the i^{th} point, s_i , is related to the z coordinate of the i^{th} point by:

$$s_i = t_s z_i; \quad (45)$$

since the track is referred to the tracker reference surface. The transformation from the primed to tracker coordinates is achieved with a rotation, $\underline{\underline{R}'}$, through an angle $-\beta$ and a translation, $\underline{\underline{T}'}$ from (x_0, y_0) to $(0, 0)$:

$$\begin{pmatrix} x \\ y \end{pmatrix} = \underline{\underline{T}'} + \underline{\underline{R}'} \begin{pmatrix} x' \\ y' \end{pmatrix}. \quad (46)$$

These transformations are given by:

$$\underline{\underline{R}'} = \begin{pmatrix} \cos \beta & -\sin \beta \\ \sin \beta & \cos \beta \end{pmatrix}; \text{ and} \quad (47)$$

$$\underline{\underline{T}'} = \begin{pmatrix} -x_0 \\ -y_0 \end{pmatrix}; \quad (48)$$

$$(49)$$

where:

$$\beta = \psi_0 - \frac{\pi}{2}. \quad (50)$$

4.3.2.3. Collecting space-points in the (x, y) plane

Helix pattern recognition follows the same conceptual steps as the straight-line pattern recognition described in section 4.3.2 A space-point is chosen in each of three stations, i, j and k where $k > j > i$. Ideally, $i = 1, j = 3$ and $k = 5$. However, a search of all combinations of three space-points for which

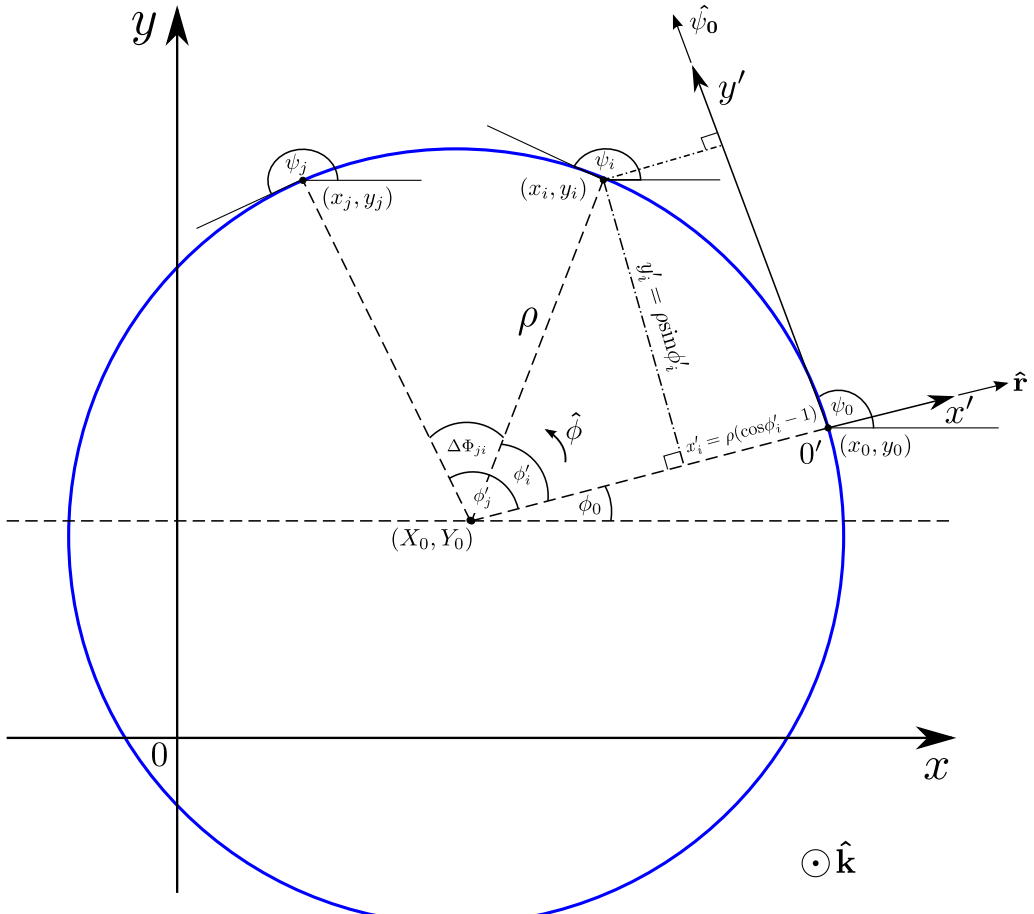


FIG. 9. Schematic diagram of track in (x, y) plane.

$k - j > 0$ and $j - i > 0$ is made, taking the combinations in the order of decreasing separation in z ; i.e. in order of decreasing $\Delta z_{kj} = z_k - z_j$ and $\Delta z_{ji} = z_j - z_i$.

A circle in the (x, y) plane may be written (see Appendix C):

$$\alpha(x^2 + y^2) + \beta x + \gamma y + \kappa = 0; \quad (51)$$

where:

$$X_0 = \frac{-\beta}{2\alpha}; \quad (52)$$

$$Y_0 = \frac{-\gamma}{2\alpha}; \quad (53)$$

$$\rho = \sqrt{\frac{\beta^2 + \gamma^2}{4\alpha^2} - \frac{\kappa}{\alpha}}; \quad (54)$$

and (X_0, Y_0) are the coordinates of the centre of the circle. Initial values for α, β, γ and κ are obtained as described in Appendix C. The distance between the x and y coordinates of the space-points in the stations l ; $l \neq i, j, k$ and the circle defined by equation 51 is given by:

$$\delta = \sqrt{(x_l - X_0)^2 + (y_l - Y_0)^2} - \rho. \quad (55)$$

In terms of the parameters α, β, γ and κ, δ may be written:

$$\delta = \sqrt{(x_l^2 + y_l^2) + \frac{\beta^2 + \gamma^2}{4\alpha^2} + \frac{\beta x_l + \gamma y_l}{\alpha}} - \sqrt{\frac{\beta^2 + \gamma^2}{4\alpha^2} - \frac{\kappa}{\alpha}}. \quad (56)$$

Points are accepted as part of a “trial” track if:

$$|\delta| < \Delta_C. \quad (57)$$

If at least one space-point satisfies this selection, a “trial track” is formed consisting of the space-points selected in stations i, j, k, \dots and l .

For each “trial track”, a circle fit is performed to calculate the fit χ_C^2 . The circle fit and expressions for the evaluation of χ_C^2 are given in Appendix ???. If χ_C^2 satisfies:

$$\frac{\chi^2}{N-3} < \chi_C^2 \text{ cut}, \quad (58)$$

then the trial track is accepted.

4.3.2.4. Collecting space-points in the (s, z) plane

The set of space points which make up the trial track provide a set of (s, z) coordinates which should lie on a straight line. Equation 45 implies:

$$s_i = \rho(\phi'_i - \phi'_0) = t_s z_i. \quad (59)$$

The angles turned through as the track propagates from station i to station j ($\Delta\Phi_{ji}$), from station j to station k ($\Delta\Phi_{kj}$) and from station i to station k are then given by:

$$\Delta\Phi_{ji} = \phi'_j - \phi'_i; \quad (60)$$

$$\Delta\Phi_{kj} = \phi'_k - \phi'_j; \text{ and} \quad (61)$$

$$\Delta\Phi_{ki} = \phi'_k - \phi'_i. \quad (62)$$

The definition of the tracker coordinate system ensures that:

$$\frac{\Delta\Phi_{ji} + 2n\pi}{\Delta z_{ji}} = \frac{\Delta\Phi_{kj} + 2m\pi}{\Delta z_{kj}} = \frac{\Delta\Phi_{ki} + 2(n+m)\pi}{\Delta z_{ki}}. \quad (63)$$

Defining:

$$\eta_{ji} = \frac{\Delta\Phi_{ji}}{\Delta z_{ji}}; \quad (64)$$

$$\eta_{kj} = \frac{\Delta\Phi_{kj}}{\Delta z_{kj}}; \text{ and} \quad (65)$$

$$\eta_{ki} = \frac{\Delta\Phi_{ki}}{\Delta z_{ki}}; \quad (66)$$

equations 63 may be inverted to yield:

$$m = \frac{\Delta z_{kj}}{2\pi} [\eta_{ji} - \eta_{kj}] + \frac{\Delta z_{kj}}{\Delta z_{ji}} n. \quad (67)$$

The correct values for n and m may now be obtained by calculating:

$$\Lambda = \eta_{ji} - \eta_{kj}; \text{ and} \quad (68)$$

$$\Gamma = \frac{2\pi}{\Delta z_{ji}} \left[m - \frac{\Delta z_{ki}}{\Delta z_{ji}} n \right]. \quad (69)$$

The most likely values of n and m for the cases of interest are $n = 0$ and $m = 0$. Therefore, searching for values of n and m for which:

$$|\Lambda - \Gamma| < \Delta_{sz}; \quad (70)$$

will yield the change in ϕ' that corresponds to a step in z .

The final step in gathering the points in (s, z) is to perform a straight line fit to the set of points corrected for multiple turns between stations. If the track fit χ^2_{sz} satisfies:

$$\chi^2_{sz} < \chi^2_{szC}; \quad (71)$$

then an attempt is made to fit a helix to the set of space points that make up the track.

4.3.2.5. Helix fit

The construction of the tracker allows the helical locus of the points on the track to be parameterised as a function of z . The step from station i to station j , a change in the z position of the track of $\Delta z_{ji} = z_j - z_i$, results in a change in ϕ' , and therefore s , where:

$$\Delta\Phi_{ji} = \frac{t_s \Delta z_{ji}}{\rho}; \text{ and} \quad (72)$$

$$\Delta s_{ji} = \rho \Delta\Phi_{ji} = \rho(\psi_j - \psi_i). \quad (73)$$

The coordinates of the track at the i^{th} station may now be written:

$$\mathbf{v}_i^{\text{hlx}} = \mathbf{v}^{\text{hlx}} + \Delta\mathbf{v}_i^{\text{hlx}}; \quad (74)$$

where:

$$\Delta\mathbf{v}_i^{\text{hlx}} = \begin{pmatrix} \Delta x_{i0} \\ \Delta y_{i0} \\ \Delta\Psi_{i0} \\ 0 \\ 0 \end{pmatrix}. \quad (75)$$

$\Delta\Psi_{i0} = \psi_i - \psi_0$ and Δx_{i0} and Δy_{i0} are obtained by evaluating:

$$\Delta x_{i0} = x_i - x_0; \text{ and} \quad (76)$$

$$\Delta y_{i0} = y_i - y_0 \quad (77)$$

where:

$$\mathbf{h}_i^{\text{hlx}} = \begin{pmatrix} x_i \\ y_i \end{pmatrix} = \underline{\underline{T}}' + \underline{\underline{R}}' \begin{pmatrix} x'_i \\ y'_i \end{pmatrix}; \quad (78)$$

and:

$$\phi'_i = \phi_0 + \Delta\Psi_{i0}. \quad (79)$$

The helix fit described in Appendix ?? procedes by minimizing:

$$\chi^2_{\text{hlx}} = \sum_i^N \left\{ \left[\mathbf{m}_i^{\text{sp}} - \mathbf{h}_i^{\text{hlx}} \right]^T \left[\underline{V}_i^{\text{sp}} \right]^{-1} \left[\mathbf{m}_i^{\text{sp}} - \mathbf{h}_i^{\text{hlx}} \right] \right\}. \quad (80)$$

If the helix fit χ^2_{hlx} satisfies:

$$\frac{\chi^2_{\text{hlx}}}{2N - 5} < \chi^2_{\text{hlxC}}; \quad (81)$$

then the trial track is accepted.

4.4. Track fit

$$\begin{pmatrix} x \\ x \\ x \\ x \\ x \end{pmatrix} = \begin{pmatrix} a & b & c & d & e \\ a & b & c & d & e \\ a & b & c & d & e \\ a & b & c & d & e \\ a & b & c & d & e \end{pmatrix} \begin{pmatrix} x \\ x \\ x \\ x \\ x \end{pmatrix} \quad (82)$$

5. Data structure

Lead author: Adam

The tracker data structure, a subset of the general MAUS data structure, is shown in figure 10. The basic unit of the MAUS data structure is the spill, representing the data produced by a single actuation of the MICE target. All MAUS modules (mappers, reducers, etc.) act on one spill at a time. The spill is then split into two sides, Monte Carlo data and reconstructed data. A key rule is that MC data must never be stored on the reconstruction side. Each side has its own event class, representing data corresponding to a single MICE particle trigger event. The relationship between the spill and the MC and recon event objects is one-to-many.

Within an MC event the only data object pertaining to the tracker is the SciFiHit, implemented as template class of the generic Hit class. This class stores the MC data used by the reconstruction to form SciFiDigits (via the map MapCppTrackerMCDigitisation). The relationship between MC events and SciFiHits is one-to-many.

On the real data side each recon event holds a single SciFiEvent (a one-to-one relationship). The SciFiEvent then holds a collection (implemented as C++ standard vectors of pointers) for each data type used in the reconstruction process: SciFiDigits, SciFiClusters, SciFiSpacePoints, SciFiStraightPRTracks, SciFiHelicalPRTracks, SciFiStraightKalmanTracks, and SciFiHelicalKalmanTracks.

6. Algorithms

Lead author: Adam

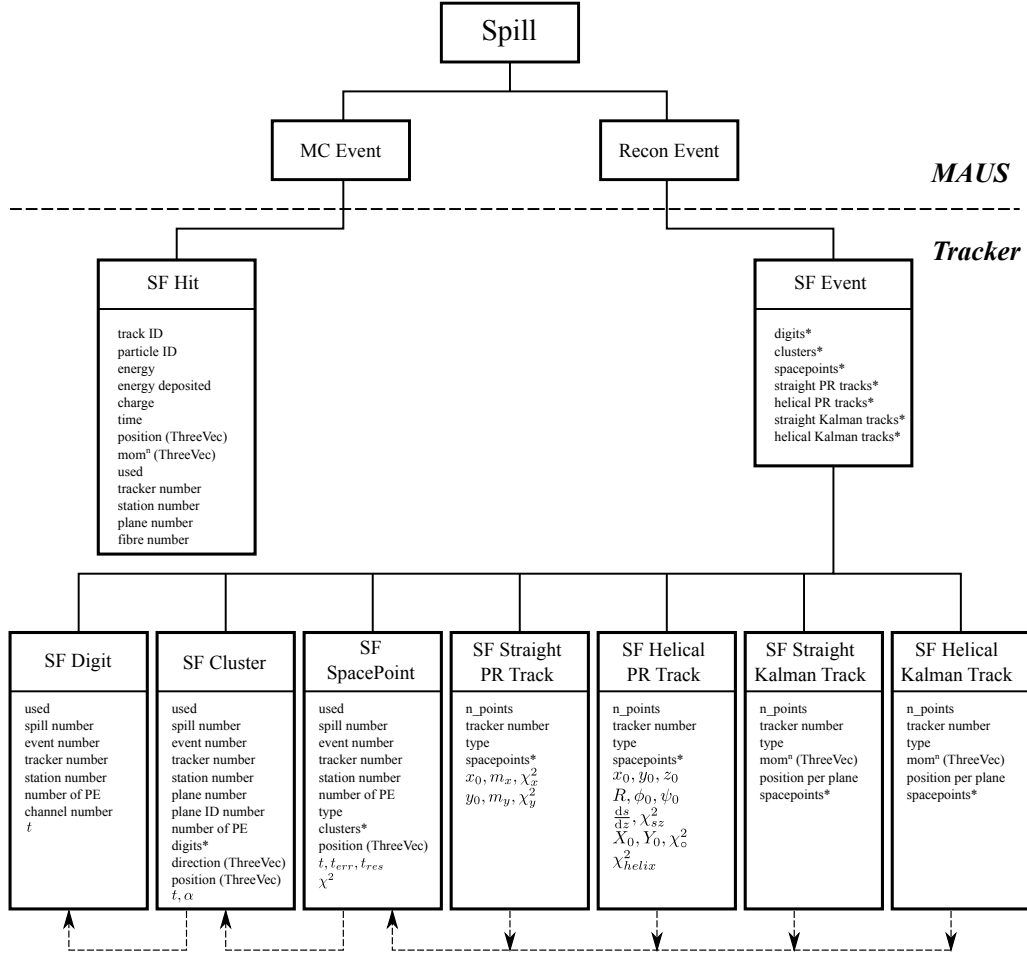


FIG. 10. The tracker data structure and its position within the general MAUS data structure. An asterisk indicates a vector of pointers. The dotted lines indicate cross links realised as vectors of pointers.

6.1. General Code Structure

MAUS operates on data using distinct modules which fall into four types: input, output, map and reduce. Input modules take data from a source and read into memory e.g. offline DAQ data, JSON files, etc. Output send data to file, e.g. ROOT or JSON. Maps perform the main work on the data, and must not perform any kind of data persistency spill to spill. Reducers are then used when it is required to accumulate data over multiple spills, e.g. to produce histograms in real time.

A diagram showing the tracker software data flow with the corresponding modules is shown in figure 11.

7. Configuration data base

Lead author: Adam

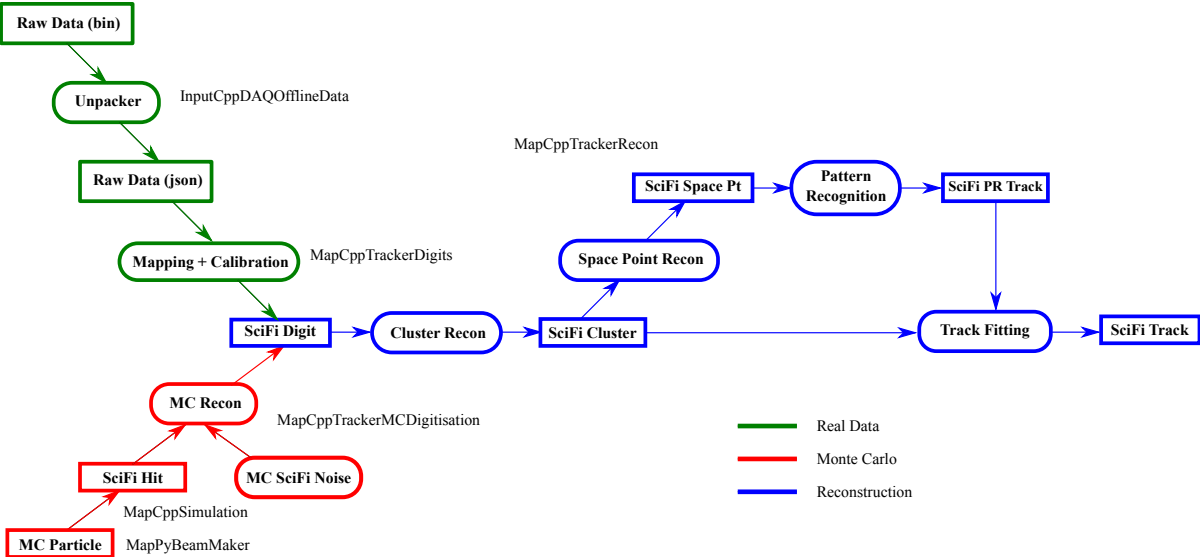


FIG. 11. Schematic of the tracker software data showing MC and Real data input, and subsequent reconstruction. MAUS modules corresponding to given process are indicated (MapCppTrackerRecon encompasses all of the reconstruction, shown in blue). Once digits have been formed, reconstruction is agnostic as to whether the MC or Real path was followed.

8. Monte Carlo

Lead author: Chris and Paul

9. Performance

Lead author: Adam, Ed and Chris

Acknowledgements

Acknowledgements.

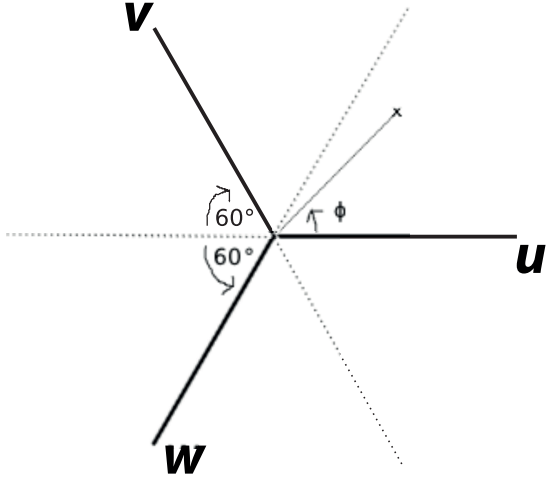


FIG. 12. Schematic representation of a point and the three plane orientations.

A. Kuno's Conjecture

For a given triplet space-point, the sum of the channel number of each cluster will be a constant.

To see how this comes about, consider the coordinate system defined by the u , v and w axes in the station reference frame shown in figure 12. The u , v and w coordinates may be written in terms of the polar coordinates (r, ϕ) as follows:

$$u = r \cos[\phi] \quad (\text{A1})$$

$$v = r \cos \left[\frac{2\pi}{3} - \phi \right] \quad (\text{A2})$$

$$w = r \cos \left[\frac{4\pi}{3} - \phi \right] \quad (\text{A3})$$

The sum $u + v + w$ may now be written:

$$u + v + w = r \left\{ \cos \phi + \cos \left[\frac{2\pi}{3} - \phi \right] + \cos \left[\frac{4\pi}{3} - \phi \right] \right\} \quad (\text{A4})$$

$$= r \left\{ \cos \phi + \left[\cos \left(\frac{2\pi}{3} \right) \cos \phi + \sin \left(\frac{2\pi}{3} \right) \sin \phi \right] + \right. \quad (\text{A5})$$

$$\left. \left[\cos \left(-\frac{2\pi}{3} \right) \cos \phi + \sin \left(-\frac{2\pi}{3} \right) \sin \phi \right] \right\} \quad (\text{A6})$$

$$= r \left\{ \cos \phi + 2 \cos \left(\frac{2\pi}{3} \right) \cos \phi \right\} \quad (\text{A7})$$

$$= r \{ \cos \phi + [-\cos \phi] \} \quad (\text{A8})$$

$$= 0 \quad (\text{A9})$$

If the sum is performed using the fibre numbers for the channels hit, the sum of the three views will equal the sum of the central-fibre numbers, i.e. if the central fibre numbers of each of the u , v and w doublet-layers is 106.5, then the sum of channel numbers will be $106.5 + 106.5 + 105.5 = 318.5$.

B. Space-point variance

Figure 13 shows the arrangement of the fibre channels in the tracker. The regions in which a space point will be reconstructed are shown by the shaded areas. The area of the triangular intersection is given by:

$$A = 4 \frac{1}{2} \frac{c_p}{\sqrt{3}} \frac{c_p}{2} \quad (\text{B1})$$

$$= \frac{c_p^2}{\sqrt{3}}; \quad (\text{B2})$$

where c_p is the channel pitch. Therefore, for the triangular intersection, the mean values of x and y are given by:

$$\bar{x} = \frac{1}{A} \int \int x dx dy \quad (\text{B3})$$

$$= \frac{1}{A} \int_0^{c_p} x dx \int_{-\frac{x}{\sqrt{3}}}^{\frac{x}{\sqrt{3}}} dy \quad (\text{B4})$$

$$= \frac{1}{A} \frac{2}{\sqrt{3}} \int_0^{c_p} x^2 dx \quad (\text{B5})$$

$$= \frac{1}{A} \frac{2}{\sqrt{3}} \frac{c_p^3}{3} \quad (\text{B6})$$

$$= \frac{\sqrt{3}}{c_p^2} \frac{2}{\sqrt{3}} \frac{c_p^3}{3} \quad (\text{B7})$$

$$= \frac{2}{3} c_p; \text{ and} \quad (\text{B8})$$

$$\bar{y} = \frac{1}{A} \int \int y dx dy \quad (\text{B9})$$

$$= \frac{1}{A} \int_0^{c_p} dx \int_{-\frac{x}{\sqrt{3}}}^{\frac{x}{\sqrt{3}}} y dy \quad (\text{B10})$$

$$= \frac{1}{A} \int_0^{c_p} \left[\frac{y^2}{2} \right]_{-\frac{x}{\sqrt{3}}}^{\frac{x}{\sqrt{3}}} dx \quad (\text{B11})$$

$$= 0. \quad (\text{B12})$$

The variance of the x and y coordinates are then given by:

$$V_x = \sigma_x^2 = \frac{1}{A} \int \int (x - \bar{x})^2 dx dy \quad (\text{B13})$$

$$= \frac{1}{A} \int_0^{c_p} dx \int_{-\frac{x}{\sqrt{3}}}^{\frac{x}{\sqrt{3}}} (x - \bar{x})^2 dy \quad (\text{B14})$$

$$= \frac{1}{A} \frac{2}{\sqrt{3}} \int_0^{c_p} x(x - \bar{x})^2 dx \quad (\text{B15})$$

$$= \frac{1}{A} \frac{2}{\sqrt{3}} \int_0^{c_p} (x^3 - 2x^2 \bar{x} + \bar{x}^2 x) dx \quad (\text{B16})$$

$$= \frac{1}{A} \frac{2}{\sqrt{3}} \int_0^{c_p} (x^3 - \frac{4}{3} c_p x^2 + \frac{4}{9} c_p^2 x) dx \quad (\text{B17})$$

$$= \frac{1}{A} \frac{2}{\sqrt{3}} \left[\frac{x^4}{4} - \frac{4}{9} c_p x^3 + \frac{2}{9} c_p^2 x^2 \right]_0^{c_p} \quad (\text{B18})$$

$$= \frac{c_p^4}{A} \frac{2}{\sqrt{3}} \left[\frac{1}{4} - \frac{4}{9} + \frac{2}{9} \right] \quad (\text{B19})$$

$$= \frac{c_p^4}{A} \frac{2}{\sqrt{3}} \left[\frac{1}{4} - \frac{2}{9} \right] \quad (\text{B20})$$

$$= \frac{c_p^4 \sqrt{3}}{c_p^2} \frac{2}{\sqrt{3}} \frac{1}{36} \quad (\text{B21})$$

$$= \frac{1}{18} c_p^2 \quad (\text{B22})$$

$$V_x = \sigma_x^2 = \left(\frac{c_p}{3\sqrt{2}} \right)^2 ; \quad (\text{B23})$$

$$V_y = \sigma_y^2 = \frac{1}{A} \int_0^{c_p} dx \int_{-\frac{x}{\sqrt{3}}}^{\frac{x}{\sqrt{3}}} (y - \bar{y})^2 dy \quad (\text{B24})$$

$$= \frac{1}{A} \int_0^{c_p} \left[\frac{y^3}{3} \right]_{-\frac{x}{\sqrt{3}}}^{\frac{x}{\sqrt{3}}} dy \quad (\text{B25})$$

$$= \frac{1}{A} \frac{2}{3\sqrt{3}} \int_0^{c_p} x^3 dx \quad (\text{B26})$$

$$= \frac{1}{A} \frac{2}{9\sqrt{3}} \left[\frac{x^4}{4} \right]_0^{c_p} \quad (\text{B26})$$

$$= \frac{1}{A} \frac{2}{9\sqrt{3}} \frac{c_p^4}{4} \quad (\text{B27})$$

$$= \frac{\sqrt{3}}{c_p^2} \frac{2}{9\sqrt{3}} \frac{c_p^4}{4} \quad (\text{B28})$$

$$= \frac{1}{9} \frac{c_p^2}{2} \quad (\text{B29})$$

$$= \frac{1}{18} c_p^2 \quad (\text{B30})$$

$$V_y = \sigma_y^2 = \left(\frac{c_p^2}{3\sqrt{2}} \right)^2 . \quad (\text{B31})$$

The covariance is given by:

$$V_{xy} = \frac{1}{A} \int \int (x - \bar{x})(y - \bar{y}) dx dy \quad (\text{B32})$$

$$= \frac{1}{A} \int_0^{c_p} (x - \bar{x}) dx \int_{-\frac{x}{\sqrt{3}}}^{\frac{x}{\sqrt{3}}} (y - \bar{y}) dy \quad (\text{B33})$$

$$= \frac{1}{A} \int_0^{c_p} (x - \bar{x}) \left[\frac{1}{2} y^2 - y \bar{y} \right]_{-\frac{x}{\sqrt{3}}}^{\frac{x}{\sqrt{3}}} \quad (\text{B34})$$

$$= 0. \quad (\text{B35})$$

Therefore:

$$\sigma_x = \sigma_y = \frac{c_p}{3\sqrt{2}} = 384.4 \mu\text{m}. \quad (\text{B36})$$

For the hexagonal case, the area of the overlapping region (shaded zone in the right panel of figure 13) is given by:

$$A = 6 \frac{1}{2} \frac{c_p}{\sqrt{3}} \frac{c_p}{2} \quad (\text{B37})$$

$$= \frac{\sqrt{3}}{2} c_p^2. \quad (\text{B38})$$

By symmetry, $\bar{x} = \bar{y} = 0$. The variance of the x and y coordinates are given by:

$$V_x = \sigma_x^2 = \sigma_y^2 = \frac{1}{A} \int \int (x - \bar{x})^2 dx dy \quad (\text{B39})$$

$$= \frac{1}{A} \int \int x^2 dx dy \quad (\text{B40})$$

$$= \frac{2}{A} \int_{-\frac{c_p}{2}}^0 x^2 dx \int_{-\frac{x}{\sqrt{3}} - \frac{c_p}{\sqrt{3}}}^{\frac{x}{\sqrt{3}} + \frac{c_p}{\sqrt{3}}} dy \quad (\text{B41})$$

$$= \frac{2}{A} \int_{-\frac{c_p}{2}}^0 x^2 \left[2 \left(\frac{x}{\sqrt{3}} + \frac{c_p}{\sqrt{3}} \right) \right] dx \quad (\text{B42})$$

$$= \frac{2}{A} \frac{2}{\sqrt{3}} \int_{-\frac{c_p}{2}}^0 (x^3 + x^2 c_p) dx \quad (\text{B43})$$

$$= \frac{2}{A} \frac{2}{\sqrt{3}} \left[-\frac{1}{4} \frac{c_p^4}{16} + \frac{1}{3} \frac{c_p^4}{8} \right]_{-\frac{c_p}{2}}^0 \quad (\text{B44})$$

$$= \frac{2}{A} \frac{2}{\sqrt{3}} \left[\frac{1}{8} \left(\frac{1}{3} - \frac{1}{8} \right) c_p^4 \right] \quad (\text{B45})$$

$$= \frac{2}{A} \frac{2}{\sqrt{3}} \frac{1}{8} \frac{5}{24} c_p^4 = \frac{1}{A} \frac{5}{48\sqrt{3}} c_p^4 \quad (\text{B46})$$

$$= \frac{2}{\sqrt{3} c_p^2} \frac{5}{48\sqrt{3}} c_p^4 = \frac{2}{\sqrt{3}} \frac{5}{48\sqrt{3}} c_p^2 \quad (\text{B47})$$

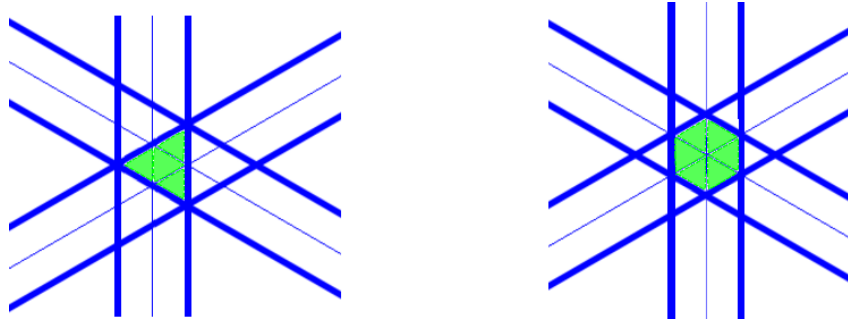


FIG. 13. Right panel: Fibre arrangement in station 5 of tracker 1. Left panel: Fibre arrangement in the rest of the stations. The shaded region shows the intersection of the three channels is triangle for every station other than station 5, where it will be an hexagon.

As before, the covariance is given by:

$$V_{xy} = \frac{1}{A} \int \int (x - \bar{x})(y - \bar{y}) dx dy \quad (\text{B48})$$

$$\begin{aligned} &= \frac{2}{A} \int_{-\frac{c_p}{2}}^0 x dx \int_{-\frac{x}{\sqrt{3}} - \frac{c_p}{\sqrt{3}}}^{\frac{x}{\sqrt{3}} + \frac{c_p}{\sqrt{3}}} y dy \\ &= \frac{2}{A} \int_{-\frac{c_p}{2}}^0 x dx \left[\frac{1}{2} y^2 \right]_{-\frac{x}{\sqrt{3}} - \frac{c_p}{\sqrt{3}}}^{\frac{x}{\sqrt{3}} + \frac{c_p}{\sqrt{3}}} \\ &= 0. \end{aligned} \quad (\text{B49})$$

Therefore:

$$\sigma_x = \sigma_y = \sqrt{\frac{5}{2} \frac{c_p}{6}} = 429.8 \mu\text{m}. \quad (\text{B50})$$

C. Circle parameters from three points

A circle in the plane $z = 0$ may be parameterised as:

$$(x - X_0)^2 + (y - Y_0)^2 = \rho^2; \quad (\text{C1})$$

where (X_0, Y_0) is the position of the centre of the circle and ρ is its radius. Expanding:

$$(x^2 + y^2) - 2X_0x - 2Y_0y = \rho^2 - (X_0^2 + Y_0^2); \quad (\text{C2})$$

which implies:

$$\frac{(x^2 + y^2)}{\rho^2 - (X_0^2 + Y_0^2)} - \frac{2X_0x}{\rho^2 - (X_0^2 + Y_0^2)} - \frac{2Y_0y}{\rho^2 - (X_0^2 + Y_0^2)} = 1. \quad (\text{C3})$$

The circle may be parameterised:

$$\alpha(x^2 + y^2) + \beta x + \gamma y + \kappa = 0; \quad (\text{C4})$$

where:

$$\alpha = \frac{1}{\rho^2 - (X_0^2 + Y_0^2)}; \quad (C5)$$

$$\beta = -2X_0\alpha; \quad (C6)$$

$$\gamma = -2Y_0\alpha; \quad (C7)$$

$$\kappa = -1. \quad (C8)$$

These equations are readily inverted to yield:

$$X_0 = \frac{-\beta}{2\alpha}; \quad (C9)$$

$$Y_0 = \frac{-\gamma}{2\alpha}; \quad (C10)$$

$$\rho = \sqrt{\frac{\beta^2 + \gamma^2}{4\alpha^2} - \frac{\kappa}{\alpha}}. \quad (C11)$$

The equation of a circle passing through three points (x_i, y_i) , where $i = 1, 2, 3$ can be found from:

$$\begin{vmatrix} x^2 + y^2 & x & y & 1 \\ x_1^2 + y_1^2 & x_1 & y_1 & 1 \\ x_2^2 + y_2^2 & x_2 & y_2 & 1 \\ x_3^2 + y_3^2 & x_3 & y_3 & 1 \end{vmatrix} = 0; \quad (C12)$$

which can be re-written as:

$$(x^2 + y^2) \begin{vmatrix} x_1 & y_1 & 1 \\ x_2 & y_2 & 1 \\ x_3 & y_3 & 1 \end{vmatrix} - x \begin{vmatrix} x_1^2 + y_1^2 & y_1 & 1 \\ x_2^2 + y_2^2 & y_2 & 1 \\ x_3^2 + y_3^2 & y_3 & 1 \end{vmatrix} + y \begin{vmatrix} x_1^2 + y_1^2 & x_1 & 1 \\ x_2^2 + y_2^2 & x_2 & 1 \\ x_3^2 + y_3^2 & x_3 & 1 \end{vmatrix} - \begin{vmatrix} x_1^2 + y_1^2 & x_1 & y_1 \\ x_2^2 + y_2^2 & x_2 & y_2 \\ x_3^2 + y_3^2 & x_3 & y_3 \end{vmatrix} = 0. \quad (C13)$$

Comparing this relation with equation C4:

$$\alpha = \begin{vmatrix} x_1 & y_1 & 1 \\ x_2 & y_2 & 1 \\ x_3 & y_3 & 1 \end{vmatrix} \quad (C14)$$

$$\beta = - \begin{vmatrix} x_1^2 + y_1^2 & y_1 & 1 \\ x_2^2 + y_2^2 & y_2 & 1 \\ x_3^2 + y_3^2 & y_3 & 1 \end{vmatrix} \quad (C15)$$

$$\gamma = \begin{vmatrix} x_1^2 + y_1^2 & x_1 & 1 \\ x_2^2 + y_2^2 & x_2 & 1 \\ x_3^2 + y_3^2 & x_3 & 1 \end{vmatrix} \quad (C16)$$

$$\kappa = - \begin{vmatrix} x_1^2 + y_1^2 & x_1 & y_1 \\ x_2^2 + y_2^2 & x_2 & y_2 \\ x_3^2 + y_3^2 & x_3 & y_3 \end{vmatrix}. \quad (C17)$$

Noting that:

$$(x + \frac{\beta}{2\alpha})^2 + (y + \frac{\gamma}{2\alpha})^2 = \left(\sqrt{\frac{\beta^2 + \gamma^2}{4\alpha^2} - \frac{\kappa}{\alpha}} \right)^2. \quad (C18)$$

the position of the centre of the circle, (X_0, Y_0) and its radius, ρ , are given by equations C9 to C11.

D. Circle fit